AN EXPERIMENTAL INVESTIGATION ON THE DYNAMIC RESPONSE VARIABILITY OF A TURBINE BLADE WITH MID-SPAN DAMPERS

Proceedings of ASME Turbo Expo 2022
Turbomachinery Technical Conference and Exposition
GT2022
June 13-17, 2022, Rotterdam, The Netherlands

GT2022-79980

AN EXPERIMENTAL INVESTIGATION ON THE DYNAMIC RESPONSE VARIABILITY OF A TURBINE BLADE WITH MID-SPAN DAMPERS

Erhan Ferhatoglu*, Daniele Botto*, Stefano Zucca*

* Department of Mechanical and Aerospace Engineering, Politecnico di Torino, Italy

ABSTRACT

This paper addresses two main subjects. Firstly, a novel test setup is described to experimentally study the nonlinear dynamic behavior of a turbine blade coupled with two mid-span dampers. To this end, a representative turbine blade and mid-span friction dampers are originally designed, and they are assembled to a special test rig which has been previously developed at Politecnico di Torino. Secondly, the variability of the dynamic response is intensively investigated with a purposely defined loading/unloading strategy. To better understand the inherent kinematics of the blade-damper interaction, contact forces are measured through the novel design of the experimental campaign. It is shown that multiple responses, which are obtained in different tests while keeping all user-controlled inputs nominally same, are due to non-unique contact forces that provide different static force equilibria on the damper. This outcome is further supported by the qualitative illustration of hysteresis cycles. The current study contributes to the understanding of the response repeatability linked to the non-uniqueness of friction forces.

Keywords: Nonlinear Response, Non-unique Friction Forces, Uncertainty Quantification, Contact Force

1. INTRODUCTION

Turbine bladed disks may be exposed to large oscillations that could cause high cycle fatigue failure in service [1, 2]. Vibration mitigation with friction damping is one of the solution techniques to extend their longevity. In this regard, different types of friction dampers are successfully used in turbo machinery applications, as an auxiliary structure to dissipate the excessive energy [3-7].

Mid-span damper (MSD) is a special type of dampers, utilized in the last stage blades of steam turbines [8-11]. MSDs are solid and metallic components coupled to blades approximately 70% above from the root. They are highly capable of reducing vibration amplitudes of last stage blades, as demonstrated in [8-11]. Apart from the effectiveness of MSDs on the energy dissipation; it has also been shown in [11] that the vibration response of the blade is not unique, and multiple solutions exist, even though all user-controlled inputs have been identical. The authors of [11] have stated that "*the nonlinear vibration response in the MSD applications may vary considerably under the same nominal conditions, due to an uncertainty related to the non-uniqueness of friction forces*"; but, this observation could not have been demonstrated in [11] with an experimental data, since it was only based on computational simulations.

The variability of the nonlinear dynamic response of structures including frictional components creates a challenge for researchers in interpreting the results reasonably. To explain the underlying reason of obtaining non-repeatable data, some of the tribological studies have focused on the effect of asperities [12] and roughness [13] of the surfaces. It has been revealed that the real touching area on the contact pairs has significant importance on the frictional behavior. In some other studies, the variability phenomenon has been associated to several uncertainties present at the contact interfaces [14, 15]. Interested readers may refer to [16] for a more comprehensive review. On the other side, the number of experimental works trying to reveal the main argument leading to multiple responses is scarce in turbomachinery applications with dampers; because, the variability phenomenon requires a highly dedicated test rig that enables the investigation of damper kinematics and the measurement of internal contact forces. Conventional designs with one damper pressed in between two adjacent blades [17, 18] are mostly for collecting the forced response data. These test structures are efficient to study the dissipation capabilities of the dampers during the in-phase and out-of-phase motions, but they do not give inherent dynamics on the lack of response repeatability.

In this paper, a novel test setup is developed to experimentally investigate the root cause of the variability phenomenon in an academic turbine blade with mid-span dampers. The main architecture of this study is inspired by an experimental campaign originally developed for a blade with

under-platform dampers in [19]. The test rig of the current work is basically an assembly of one central blade, two mid-span dampers, and auxiliary components that enable the measurement of contact forces as well as the dynamic response of the blade. In the experiments, multiple responses are obtained in different runs with a purposely defined loading/unloading sequence while keeping the user-controlled inputs nominally same. It should be noted that there may be several factors influencing the repeatability of the tests, and it is impossible to keep all of them under the user control. The main motivation of the current strategy is to ensure macro scale conditions as similar as possible for different runs, and then to identify the dominant varying parameter causing the non-repeatability in the tests. In accordance with this purpose, a large number of case studies with various harmonic excitation levels and pre-loads are intensively examined. The damper kinematics is also monitored with a differential laser by recording the rotational motion of the damper and the relative displacements between the bodies. It is shown that the experimental results are highly consistent with the argument made in [11] stating that the variability in the vibration response amplitudes is due to an uncertainty related to the non-uniqueness of friction forces. It is demonstrated that this phenomenon provides different static balances on the damper under the same nominal conditions, which, in turn, leads to the response variability. To the best of authors' knowledge, this study presents the first experimental investigation explaining the effects of the non-uniqueness of friction forces on the dynamic response variability. Moreover, a novel test setup is presented for the first time in the experimental characterization of the dynamic behavior of turbine blades coupled with mid-span dampers.

The paper is organized as follows. Section 2 introduces the test setup and describes the measurement procedures. Section 3 presents and discusses the results. Section 4 summarizes and concludes the paper.

2. EXPERIMENTAL CAMPAIGN

2.1 Description of the Test Setup

The entire test rig is a large assembly composed of three main substructures. Figure 1a depicts the complete picture of the test setup.

The first substructure consists of one central and two side blocks, which form the main frame of the test rig. The central block has a clamping mechanism inside. Basically, it applies a large static force (F_{CLAMP}) from the bottom and sticks the blade root to its female fir-tree slot. In this way, a possible source of friction at the blade root is prevented. Side blocks are bulky entities that are bolted to the table. They carry auxiliary components on themselves to measure contact forces. One of the components is an L-shaped force de-coupler. This element distributes the reaction forces (R) in two perpendicular directions. The forces are then measured by a load cell (LC) that is attached between the de-couplers and the side blocks.

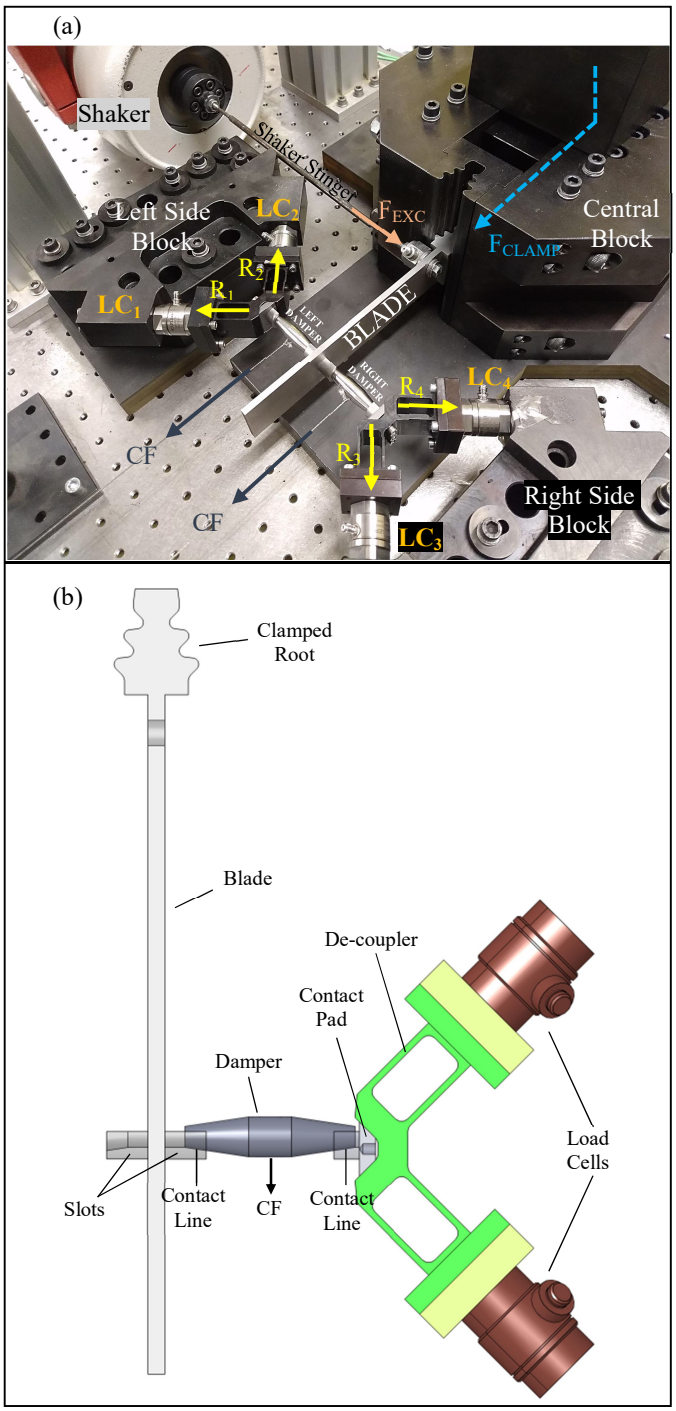

FIGURE 1: (a) A VIEW OF THE ASSEMBLED TEST SETUP, (b) A TOP VIEW OF MODELS FOR THE RIGHT SIDE

This first substructure has been already manufactured previously at Politecnico di Torino, and it has been used in [19]. The details about the design of these parts and the clamping mechanism can be extensively found in [19]. They are not given here for brevity.

The second substructure is the blade itself. It imitates the last stage blades of steam turbines utilized in industrial applications [8-11], and it is originally developed for academic purposes in this study. The top view of the blade model, together with the parts at the right side, is depicted in Figure 1b. The blade has a rectangular cross section and is a slender beam with 4 mm thickness and 160 mm length. At the mid-span of the blade, there are two cylindrical slots on which the damper can engage and come into contact with the blade. In the experiments, the blade is harmonically excited by an electromagnetic shaker (F_{EXC}), from a position close to the root (see Figure 1).

The third substructure consists of dampers and contact pads. The dampers are designed of the pin type geometry, as similar to their industrial counterparts utilized in [8-11]. They have a non-uniform cross section throughout their horizontal axes and three different portions with a total length of 40 (15+10+15) mm. The ends and the middle portion are cylindrical with 5 mm and 9.5 mm diameters, respectively. These dimensions ensure an 8.53° inclined cylindrical contact region on each side. Dead weights are applied from the middle portion of the dampers, which creates a static pre-load simulating the centrifugal force (CF) effect. The pre-load presses the dampers in between the blade and contact pads. These pads are directly bolted to the de-couplers and provide a frictional surface mimicking the contact region of a dummy adjacent blade. They have exactly the same contact regions of the slots on the real blade's mid-span. In this way, the contact surfaces become similar at each side of the damper. It should also be noted that the axes of the mating pairs are intentionally designed eccentric to ensure a line contact in the tests. This feature is an imitation of real life applications [11], implemented by making the radius of the damper curvature smaller than that of the slots and pads.

2.2 Measurement Procedures

The experiments are performed with a conventional force controlled stepped-sine methodology around the first lateral in-plane resonance region. Frequency sweeps are done by defining a lower and an upper limit in which the resonance frequency is included. The Simcenter SCADAS Mobile data acquisition system is utilized for acquiring the time signals. The sampling frequency and windowing are properly taken into account to measure the data correctly. Several parameters are recorded during the tests, and their measurement procedures are explained in the following.

The first quantity measured is the reaction forces on the load cells, from which the contact forces can be easily derived. Figure 2a depicts the force balance on the right de-coupler. R_3 and R_4 are the measured forces by load cells, while T and N represent the tangential and normal forces on the contact pad. α and θ are 45° and 8.53°, respectively, and they are design parameters of the de-coupler and the contact pad. The geometry of the components is purposely designed in such a way that forces intersect exactly at the middle point of the contact line. Thus, all forces act on the same point, and the possibility of a

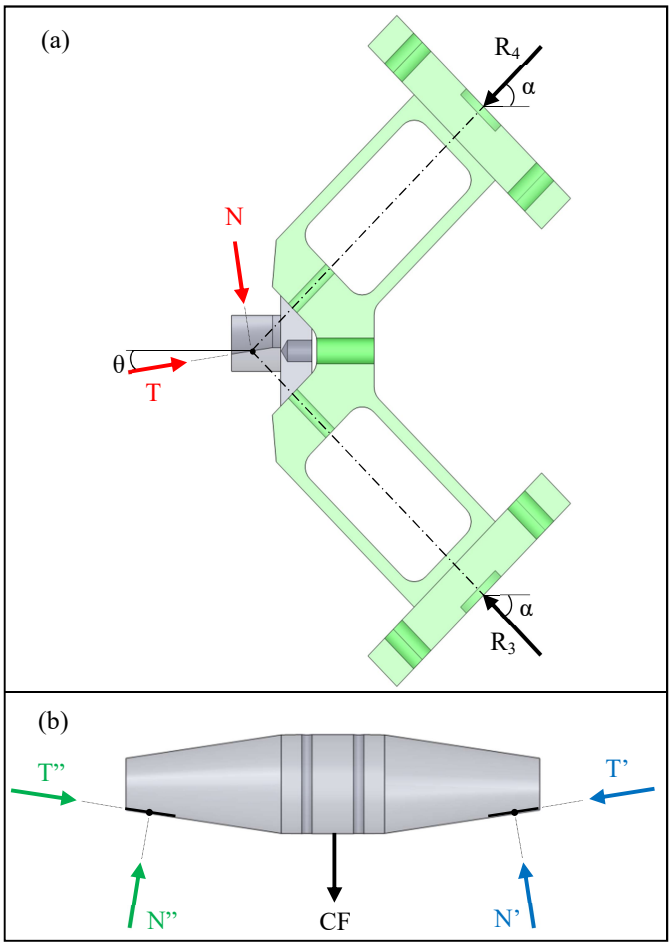

FIGURE 2: FORCE BALANCES: (a) ON THE CONTACT PAD, (b) ON THE DAMPER

moment due to a force eccentricity is prevented. The contact forces can be derived with two coupled force balances in the horizontal and vertical directions as follows

$$\begin{aligned} T\cos(\theta)+N\sin(\theta)-R_3\cos(\alpha)-R_4\cos(\alpha)=0 \\ T\sin(\theta)-N\cos(\theta)+R_3\sin(\alpha)-R_4\sin(\alpha)=0 \end{aligned} \quad (1)$$

The accuracy of this calculation method is deeply investigated in [19] with the same de-coupler mechanism by including several parameters such as the elasticity of the de-couplers or the degree of separation in forces. It has been reported that it enables an accurate measurement of contact forces with a deviation less than 1%. Figure 2b also shows the force balance achieved on the damper. T' and N' are the contact forces at the de-coupler side of the damper with the same magnitude of T and N but in opposite directions. Contact forces at the blade side, T" and N", can also be computed with force balance equations. They can be written as

$$\begin{aligned} T''\cos(\theta)+N''\sin(\theta)-T'\cos(\theta)-N'\sin(\theta)=0 \\ -T''\sin(\theta)+N''\cos(\theta)-T'\sin(\theta)+N'\cos(\theta)-CF=0 \end{aligned} \quad (2)$$

In this way, all forces on contact interfaces can be easily obtained. There are two assumptions that are worthy to mention for Eq. (2). The first one is that the bending on the damper, caused by the pre-load, is negligible. This assumption is simply confirmed with a preliminary analysis (not shown here for brevity) by assuming the damper as a simply supported beam. The static deformation is extremely small (less than 1μm), and the effects of the bending can be ignored. The second assumption is that the inertia of the damper is neglected, since the mass of the dampers are only 15.3 grams. Nevertheless, it will be numerically shown in Section 3.3.2 that the effect of the inertial forces can be safely ignored. It should also be noted that CF is applied by using steel ropes that pass through two successive pulleys. A static test is initially performed to quantify the friction between the rope and pulleys. It is measured that the actual force transmitted to the dampers is 95% of the dead weights. As a result, a correction of 0.95 is applied in the CF. The procedures of measuring contact forces on the de-coupler and the damper at the left side can be similarly followed as explained above. They are not repeated for brevity.

A differential laser is also used in the experiments while the test setup is in operation. The laser measured two different parameters to extract the inherent kinematics of the damper. The first one is the relative displacement between two ends of the damper. The laser is pointed in parallel, from the direction of the dead weights to the two positions located at both ends of the right damper, as shown in Figure 3a. The distance between the two points (h) is 20 mm. This measurement enables the prediction of the damper's rigid rotational motion around its vertical axis (see Figure 3a), with a simple geometrical relation. The second parameter measured by the laser is the relative displacement between the damper and the blade. This measurement is done to construct the hysteresis cycles. However, it should be underlined that there are limitations on the exact measurement of the relative displacement due to the lack of space in the test campaign for this particular measurement. Nevertheless, the main aim here is only to qualitatively interpret the behavior of hysteresis cycles with roughly measured relative displacements. A quantitative assessment of contact parameters is out of scope here. Figure 3b and Figure 3c show the laser points and the position of laser heads, respectively. One of the heads is directed to a point located on a close region to the contact slot of the blade, while the other head is pointed on top of the damper. Here, a reflective tape is attached via an additional indenter wrapped around the damper, since the middle portion of the damper is perfectly circular and does not have any indentation to reflect the light back to the laser. Moreover, the laser has to be inclined (around 12°-15°) to be able to take the measurements. Even though the final results cannot be assumed perfectly accurate, the authors find them illustrative for a qualitative interpretation, and worth mentioning in the paper. The last parameter recorded is the response of the blade with an accelerometer attached to the blade tip as shown in Figure 3b.

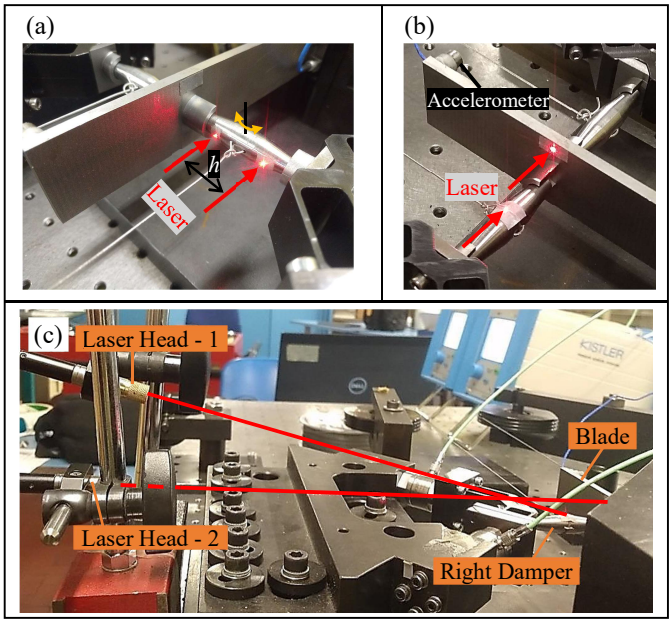

FIGURE 3: (a) LASER POINTS FOR THE ROTATIONAL MOTION,(b) LASER POINTS FOR RELATIVE DISPLACEMENTS, (c) A BACK VIEW FOR THE POSITION OF THE LASER HEADS

3. RESULTS AND DISCUSSION

3.1 Linear Response of the Blade

To characterize the blade's linear behavior, frequency sweeps are performed initially for the free blade. A sensitivity analysis is also done on the clamping force to minimize the friction introduced from the fir-tree root. In this study, F_{CLAMP} is set to a large enough value that minimizes the damping at the blade root.

The normalized response of the blade for an increasing level of excitations is shown in Figure 4a. It can be seen that the response overlaps except for the case with the lowest excitation. It is necessary to highlight the fact that it is practically impossible to completely prevent the damping at the blade root as well as the material damping in the blade, no matter how large clamping force is applied. The results depicted in Figure 4a can be assumed reasonable enough to state that the damping at the blade root is negligible. It should also be underlined that the vibration amplitudes will drastically decrease after engaging the dampers when compared to the free blade case. It will further reduce the friction at the root, and the most dominant damping will be provided from the contacts between the blade and dampers.

The response of the free blade is given with a larger frequency interval in Figure 4b. It shows that the interested mode is a well-separated one with the natural frequency measured at 122.25 Hz.

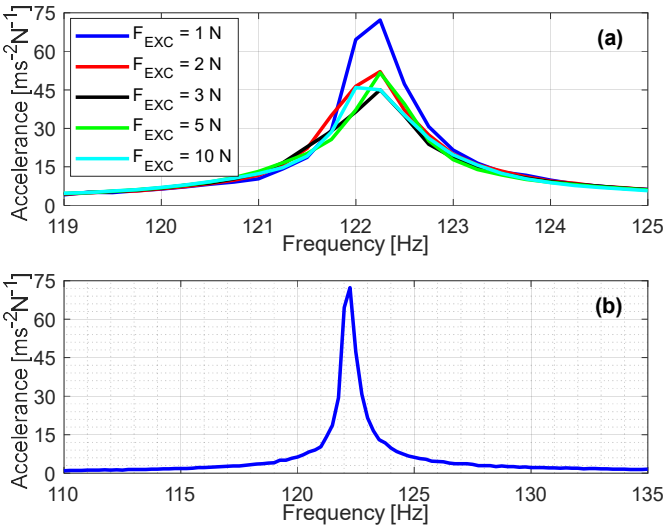

FIGURE 4: LINEAR RESPONSE OF THE BLADE WITHOUT DAMPERS

3.2 Nonlinear Response of the Blade

The nonlinear dynamic behavior of the blade coupled with the dampers is extracted with several tests. Firstly, frequency sweeps are performed with an increasing order of excitation levels, while the centrifugal forces (CF) are constant on the damper. Three dead weights (5.6 kg, 3.6 kg and 1.6 kg) are separately loaded to investigate the dissipation capability of the damper under different circumstances.

Figure 5 illustrates the normalized response amplitudes of the blade measured with various excitation levels around the first resonance region. It is obvious that the resonance frequency of the system considerably shifted to higher values when compared to the free blade case. This is due to the engaging position of mid-span dampers. They are located relatively far from the blade root, which brings a considerable amount of hardening to the system. It is clear in Figure 5 that the mid-span dampers efficiently work and reduce the vibration amplitudes of the blade by dissipating the energy. In all cases, the normalized response smoothly decreases and shows a softening behavior while the excitation increases. Moreover, the resonance region slightly shifts to the left with decreasing pre-loads, as can be seen from Figure 5a towards to Figure 5c. This observation is quite relevant; because, contact pressure on the frictional surfaces tend to increase with larger pre-loads and this ensures the increase of contact stiffness, which results in obtaining higher resonance frequencies. It is also interesting to note that the response amplitudes corresponding to the same excitation level among different cases is smaller for those obtained with low pre-loads. For instance, the response curve measured with 5 N excitation in Figure 5c is more damped than its counterpart shown in Figure 5a; because, the higher pre-load in the latter makes the response behavior closer to that of the fully stuck linear configuration.

It is worth mentioning that the direct comparison of the accelerance amplitudes shown in Figure 4 and Figure 5 can be misleading in the interpretation of the dissipative capabilities of

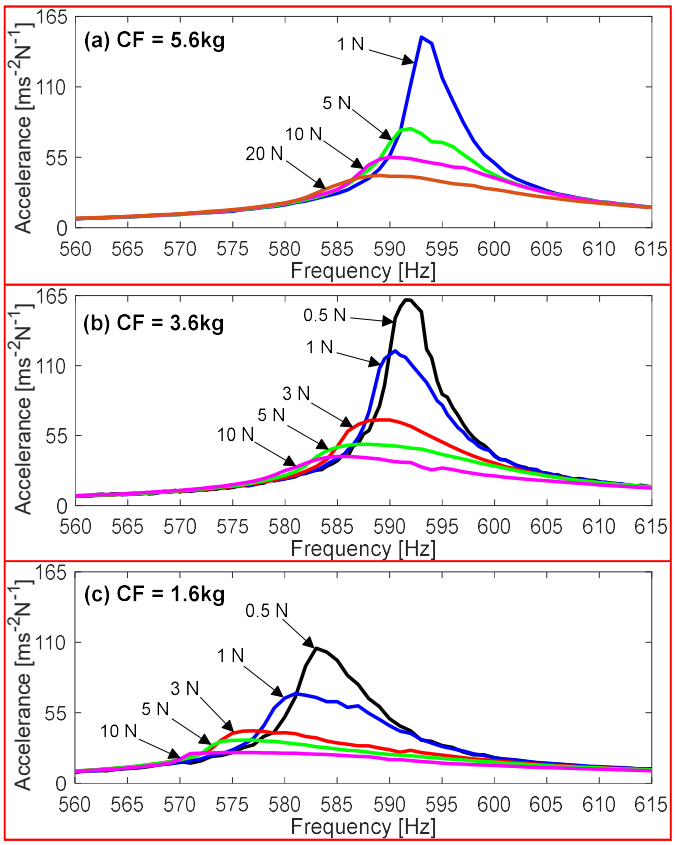

FIGURE 5: NONLINEAR RESPONSE OF THE BLADE WITH AN INCREASING ORDER OF EXCITATION LEVELS

MSDs. Some curves in Figure 5 surpass the blade's linear response shown in Figure 4, and this observation might be interpreted as the vibration level increases after engaging the dampers. It should be noted that the accelerance is a quantity obtained by the multiplication of the steady state displacement amplitude with the square of the excitation frequency. Since the resonance frequency of the coupled blade-damper configuration is approximately 5 times of the value for the stand-alone blade, the actual comparison of the displacement amplitudes should be done by dividing the values of the coupled blade-damper configuration to 25. As a result, the displacement amplitudes become much smaller with the presence of the damper, compared to the free blade case.

It is shown in each case study that the frequency sweeping strategy with an ascending order of harmonic forcing under the same pre-load gives consistent results. All observations about the nonlinear dynamic behavior of the blade coupled with mid-span dampers can be considered coherent. The next section presents the variability of the nonlinear response measured under the same nominal circumstances with purposely defined loading sequences.

3.3 The Variability of the Nonlinear Response

The variability phenomenon is a frequent occurrence in laboratory conditions. In this study, it is investigated by

following a particular testing strategy that enables the comparison of the response measured in different tests but with the same inputs.

Table 1 gives the complete picture of the experimental procedure. Before explaining the procedure, it is worth defining the terminology used in it. One complete run means a full frequency sweep with a stepped-sine approach, throughout the frequency range defined. Each run is performed with one specific pre-load and excitation level. All the measurements (nonlinear response, contact forces and relative displacements) are done simultaneously during the runs. The procedure consists of four steps. In Step 1, the excitation amplitude at which the tests will be performed is first decided, and the dampers are loaded with 6.6 kg dead weights. Step 2 consists of eight consecutive frequency runs with the defined excitation level, but different pre-loads. More specifically, in Step 2, the first run is performed with 6.6 kg. Having completed the first run, the experiment stops, and one kg dead weight is removed. The second run of the Step 2 starts again with 5.6 kg, and a full sweep is completed. The practice of decreasing pre-loads is maintained until the end of the fourth run conducted with 3.6 kg. The fifth run is again performed with 3.6 kg without touching to dead weights, and then they are gradually loaded back with one kg intervals in between the frequency sweeps, until to complete the eighth run with 6.6 kg. In step 3, the dampers are completely unloaded and reloaded back with 3.6 kg. Step 4 is accomplished with the identical logic of the second step, but with a reverse loading sequence of dead weights, i.e. they are increased first and then decreased. This approach nearly simulates the actual working environment of turbine blades in the laboratory conditions, as the centrifugal forces change with increasing and decreasing rotor speeds.

Each run takes almost one minute. The time interval between the runs is also around 15-20 seconds, which was spent for unloading/loading the dead weights and starting the next run. Thus, the entire procedure is completed in approximately 20 minutes, as there are 16 runs. This procedure gives 16 different response curves all of which are measured with the previously defined excitation level. Since four particular pre-loads are used in the tests, the curves can be separated into 4 subsets each of which contains 4 different runs corresponding to the same pre-load. As an example, the subset of 4.6 kg pre-load is composed by the 3rd, 6th, 10th and 15th runs.

TABLE 1: THE LOADING SEQUENCE OF THE DAMPERS FOR A PRESCRIBED EXCITATION LEVEL

Step 1	Step 2		Step 3	Step 4	
	Run	CF [kg]		Run	CF [kg]
Load the dampers	1	6.6	Remove and reload the dampers	9	3.6
	2	5.6		10	4.6
	3	4.6		11	5.6
	4	3.6		12	6.6
	5	3.6		13	6.6
	6	4.6		14	5.6
	7	5.6		15	4.6
	8	6.6		16	3.6

This testing strategy is applied with four different excitation amplitudes (F_{EXC}), 1 N, 3 N, 5 N and 10 N, to investigate the damper kinematics under various forcing. At the end, 16 different sets are collected with four different excitations and pre-loads. For brevity, the results are presented in six subsets with two excitation levels (1 N and 5 N) and three dead weights (3.6 kg, 4.6 kg and 6.6 kg). These subsets are shown in Table 2, and intentionally selected as demonstrators. For each subset, a parameter, which simply represents how close the system is to full stick conditions, is defined. It is computed with the ratio of CF/F_{EXC}, and normalized with respect to the first subset. It means that the highest the ratio, the closest the system is to the fully stuck configuration. In this way, different conditions in which the slip is low (Subset 1), moderate (Subsets 3, 4) and high (Subset 6) will be shown in the following. It is worth mentioning that this ratio is just an illustrative parameter that will help in the interpretation of the results.

Figure 6 depicts the frequency response curves measured around the first resonance region. To make a meaningful comparison, the results of subsets are separately given in each subfigure. Each subset contains frequency responses measured with the same inputs (F_{EXC} and CF) but in different runs as shown in Table 2. It is clear that the response is non-unique and varies in all subsets, even if all user controlled conditions at the macro scale testing environment are kept identical. This phenomenon may seem as a black box for the designers, since the response itself does not give an insight about its non-repeatability. In this study, the underlying mechanism is investigated through additional measurements thanks to the developed test rig.

3.3.1 Hysteresis Cycles

The first notable observation is that the variability is larger in some subsets. In particular, on the one hand for 1N excitation, the response behavior shows a lower variability with the highest pre-load in Figure 6a, while the scattering increases with decreasing pre-loads towards Figure 6c. On the other hand for 5 N forcing, the behavior is exactly opposite. The largest variability is obtained for 6.6 kg case in Figure 6d, and it decreases with reducing dead weights towards Figure 6f. To investigate the underlying reason why the response variability is larger in the 3rd and 4th subsets than the rest, hysteresis cycles are investigated in each test to illustrate the amount of slip.

Figure 7 depicts the hysteresis curves measured at the steady state conditions during which the system is at the corres-

TABLE 2: SUBSETS OF EXPERIMENTAL RESULTS

Subset	CF [kg]	F_{EXC} [N]	Ratio (%)	Runs
1	6.6	1	100	1, 8, 12, 13
2	4.6	1	70	3, 6, 10, 15
3	3.6	1	55	4, 5, 9, 16
4	6.6	5	20	1, 8, 12, 13
5	4.6	5	14	3, 6, 10, 15
6	3.6	5	11	4, 5, 9, 16

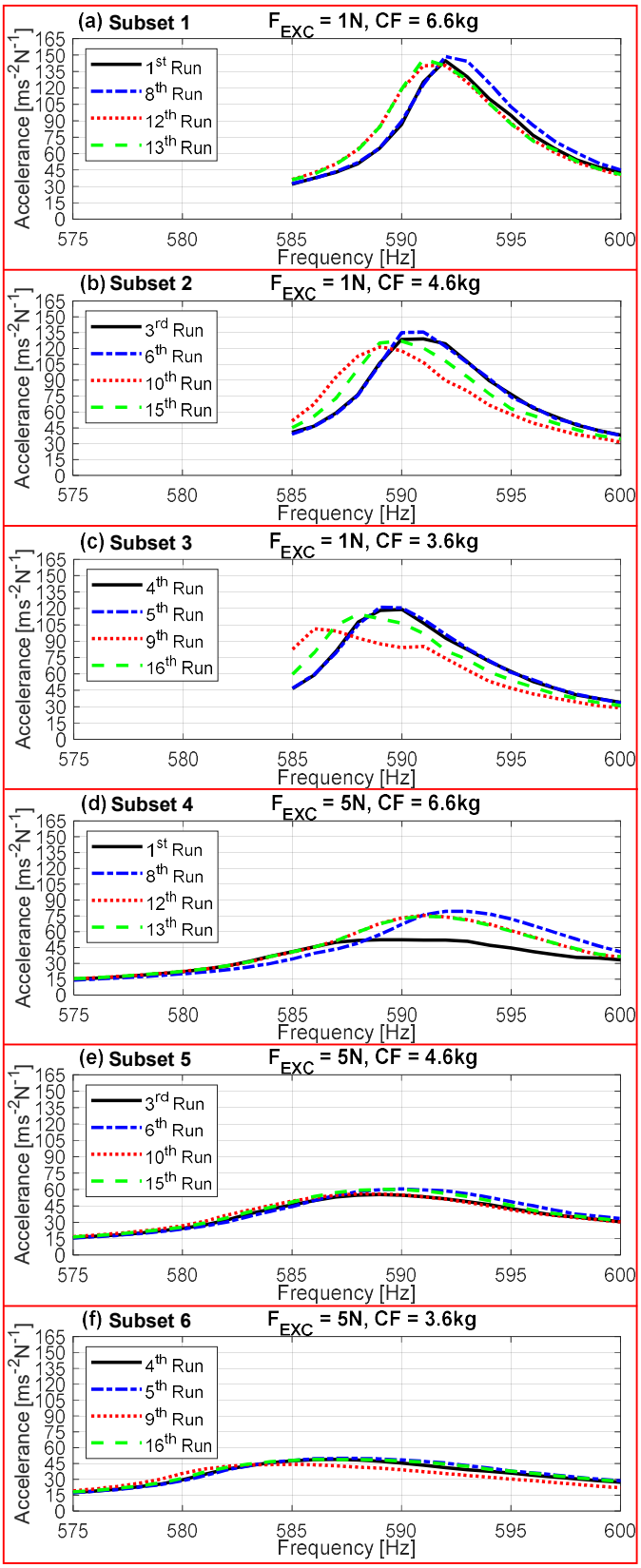

FIGURE 6: THE VARIABILITY OF NONLINEAR RESPONSE

ponding resonance frequencies. The results are presented for the 1st, 3rd, 4th and 6th subsets, to investigate the cases with the largest and lowest variability. One sample is given from each subset, for clarity. It can be noticed in Figure 7 that there is a zigzag behavior in the data; because, the differential laser struggles to smoothly measure the extremely low relative displacements (less than 0.7 μm). To ease the readability of results, hysteresis cycles are heuristically (i.e. manually) redrawn by using dotted and dashed lines. It is clear in all subsets that damping is present with a slip motion, as the inside area of the hysteresis cycles gives the dissipated energy. The shapes of the hysteresis curves indicate that micro slip occurs in all subsets. To check whether the gross slip is also achieved, the ratio of tangential forces to normal ones (T/N) is investigated. During the gross slip, the ratio is expected to be a constant value (coefficient of friction); but, it does not reach this limit (not shown here for brevity), indicating that gross slip is never achieved in the experiments.

In Figure 7a, the hysteresis shape of the 1st subset (F_{EXC} = 1 N, CF = 6.6 kg) has clearer stick region with more straight lines, while the curve of the 3rd subset (F_{EXC} = 1 N, CF = 3.6 kg) has more uncertain stick-to-slip transition region. This indicates that the micro slip in the 1st subset is less dominant than that in the 3rd. The amount of the slip in the former is also slightly less. These observations are relevant, because the 1st subset is the one closest to the fully stuck configuration among all cases, since it includes the lowest excitation (1 N) and the

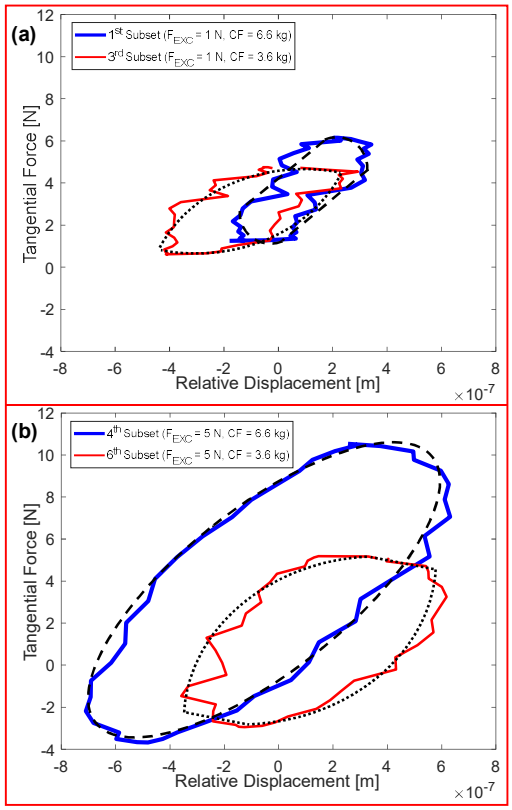

FIGURE 7: HYSTERESIS CYCLES

highest pre-load (6.6 kg), as also shown in Table 2 with the ratio of CF/F_{EXC}. Regarding 5 N excitation in Figure 7b, the shapes of the hysteresis cycles show that the motion of the damper approaches to a near gross slip in both subsets. It is interesting to note that the micro slip in the 4th subset is more dominant than the 6th one. This observation is also relevant; because, the 6th subset is the one closest to the gross slip conditions, with the lowest pre-load (3.6 kg) and the highest excitation level (5 N) among the presented subsets.

All these observations show that there is a link with the amount of micro slip and the response variability in the system. Indeed, once the micro slip is the dominating motion in the contacts, i.e. the 3rd and 4th subsets, the variability is larger as shown in Figure 6c and Figure 6d. The repeatability of the response increases towards to the fully stuck (the 1st subset) or gross slip (the 6th subset) conditions, as the response approaches to a unique one as shown in Figure 6a and Figure 6f. This observation is fully consistent with the hypothesis that the response variability is caused by the non-uniqueness of friction forces [20, 21]. According to this idea, the response may vary considerably if a dominating micro slip behavior occurs in the contacts, due to the uncertainty present in the static component of the tangential forces. It also states that the response of the system should be unique during the gross slip or fully stuck contact behavior, as observed in a similar manner in the experiments of the current work. This is the first indication that the variability in our experiments is caused by the non-uniqueness of friction forces. If there was one another main factor dominant on the response variability in the tests, it would have affected all the data regardless of the contact conditions.

3.3.2 Rigid Rotation of the Damper

Accuracy of the measured contact forces and the relative displacement between the damper and the blade may be affected by the rigid rotation of the damper around its vertical axis, which is also indirectly measured as shown in Figure 3a. However, this quantity is recorded with additional tests separately, since the laser orientation had to be changed from the previous one used for the measurement of the relative displacement between the blade and the damper.

In the experiments, the measured quantity is the relative displacement (referred to as Δd), whose amplitude is measured in the range of 1-2 μm, between the directed points of the laser. The distance between the laser measuring points (h) on the damper is 20 mm (see Figure 3a). Hence, the angle of the rotation can be estimated with a simple geometrical formulation, as $\tan^{-1}[\Delta d/h]$. Figure 8 shows directly the computed angle of the damper rotation, measured with two different pre-loads and the highest two excitation levels, for one full vibration cycle at the corresponding resonance frequency. It can be seen that even the maximum angle of the rotation is considerably small (less than $6\text{x}10^{-3}$ degrees). The inertia force (F_i) due to maximum amplitude of the damper rotation ($\theta \approx 6\text{x}10^{-3}$ deg $\approx 1.05\text{x}10^{-4}$ rad) is also computed at the resonance frequency ($\omega \approx 590$ Hz) as the multiplication of mass moment of inertia of the damper ($I \approx 1490$ g·mm^2, calculated by the de-

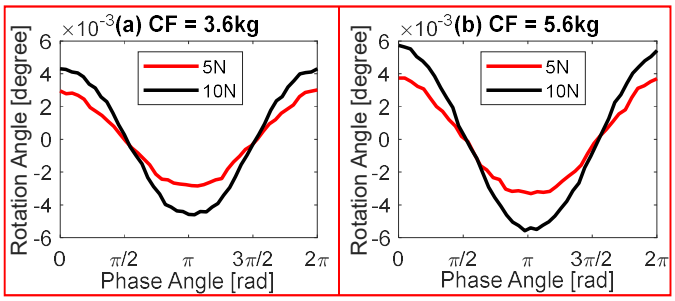

FIGURE 8: THE ANGLE OF THE DAMPER ROTATION

sign software) with the angular acceleration ($\ddot{\theta}$),

$$F_i = I\ddot{\theta} = I\omega^2\theta \approx (1490\times10^{-9})(2\pi\times590)^2(1.05\times10^{-4}) \approx 0.002\,\text{N} \quad (3)$$

The amount of the rotation angle and the computed inertia force proves that the rigid rotation of the damper is negligible and can be safely ignored.

3.3.3 Non-unique Contact Forces

Measurement of the contact forces gives an ability to interpret the inherent kinematics of the damper and the dynamics of the system. To better understand the underlying reason of the response variability, contact forces measured in each run of the subsets are directly compared at the corresponding resonance frequencies. The contact forces will be shown for the time intervals in which the force equilibrium is achieved on the de-coupler and damper at steady state. For brevity, three subsets are particularly selected for the demonstration purposes. Two of them are the ones in which the variability is the largest with the dominating micro slip behavior (the 3rd and 4th subsets, see Figure 6c and Figure 6d), while the third one has the lowest variability with a near gross slip motion (the 6th subset, see Figure 6f). In this way, it is expected that the main factor that causes the response variability will be identical for the overlapping response curves, while the same factor should differ for non-overlapping ones.

The 4th subset (F_{EXC} = 5 N, CF = 6.6 kg) is the one with the largest micro slip motion (see Figure 7b) and response variability (see Figure 6d). All contact forces on the left damper are shown for its de-coupler and blade sides in Figure 9a and Figure 9b, respectively. Moreover the upper and lower graphs of each subfigures depict the tangential and normal forces, respectively. Type and color properties of the curves are kept identical with the corresponding runs given in Figure 6d. Each graph shows the dynamic and static components together. It is worth mentioning that the static components are simply computed by averaging the dynamic part over one vibration cycle.

The first remarkable observation in Figure 9 is that dynamic components of the contact forces measured in the 1st and 8th runs are notably different from those overlapping ones

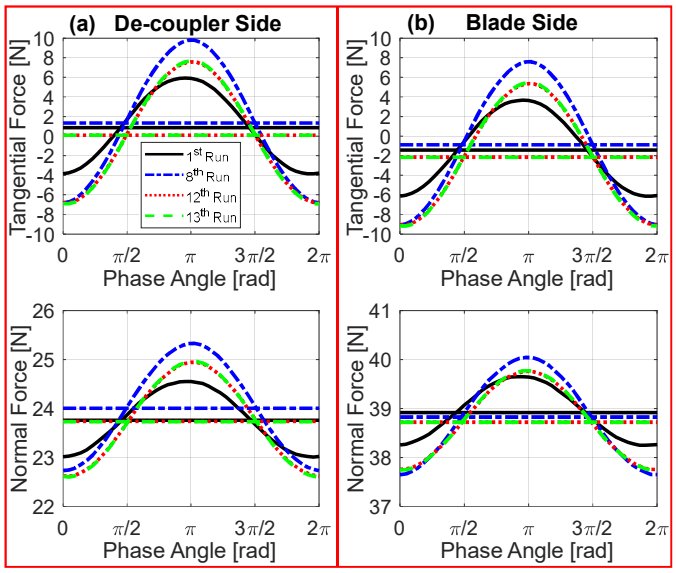

FIGURE 9: CONTACT FORCES ON THE LEFT DAMPER FOR THE 4TH SUBSET (F_{EXC} = 5 N, CF = 6.6 kg)

of the 12th and 13th runs.While the amplitude is the largest for the least damped case (the 8th run in Figure 6d), it takes its lowest value for the most damped one (the 1st run in Figure 6d). It is also in the mid-range for the overlapping responses (the 12th and 13th runs in Figure 6d). This observation is quite relevant, because it is expected from an engineering point of view that contact forces increase with higher vibration amplitudes and decrease with the lower ones.

Secondly, it can be seen that the static components are not unique, even though the applied pre-load is nominally the same for all runs. It is an indication of an uncertainty that varies the static components and, thus, enables the static force equilibrium on the damper in different ways. To better illustrate it, Table 3 numerically gives the static components of contact forces with the notations given in Figure 2b. As an example, force balance of the 1st run can be written in the horizontal (x) and vertical (y) directions with Eq. (2) as

$$F_x = (38.92 - 23.76)\sin(8.53) - (1.41 + 0.86)\cos(8.53) = 0.0038$$

and

$$F_y = (1.41 - 0.86)\sin(8.53) + (38.92 + 23.76)\cos(8.53) - 6.66 \times 9.81 \times 0.95 = 0.0004,$$

respectively. Since the resultant forces are almost 0 (the deviations are due to round-off errors), the damper is said in balance. The same procedure can be applied for the 8th, 12th and 13th runs, too, and it can be understood that the force equilibrium on the damper is non-unique. It should also be noted that this computation is just a crosscheck of Eq. (2), after obtaining the contact forces by using the same equation. Lastly, it is worthy to mention that the exact mass of the dead weight is 6.66 kg, as shown in these balance equations. Its last digit was omitted throughout the paper for simplicity. This fact applies the other dead weights, as well.

TABLE 3: STATIC COMPONENTS OF CONTACT FORCES ON THE LEFT DAMPER FOR THE 4TH SUBSET (F_{EXC} = 5 N, CF = 6.6 kg)

Runs	T'	N'	T''	N''	Resultant Force	
					X Dir.	Y Dir.
1st	0.86	23.76	-1.41	38.92	0.0038	0.0004
8th	1.33	24	-0.89	38.82	0.0028	-0.008
12th	0.097	23.73	-2.15	38.72	0.0013	-0.0042
13th	0.092	23.73	-2.16	38.72	-0.0037	-0.0019

For the sake of completeness, contact forces on the right damper for the same set are also given in Figure 10. The non-uniqueness of the static components is present on this damper, as well. The values are numerically given in Table 4 from which the non-unique force equilibria corresponding to different runs can be easily demonstrated. However, it should be noted in Figure 9 and Figure 10 that the variability pattern of the static components of the tangential forces closely matches that of the response variability shown in Figure 6d. In other words, the static tangential forces and the response of the 12th and 13th runs overlap very well in all figures; and, the curves of the 1st and 8th runs are distinct and separated from them. These observations show that there is a relation between the response variability and the corresponding non-unique static components of the tangential forces.

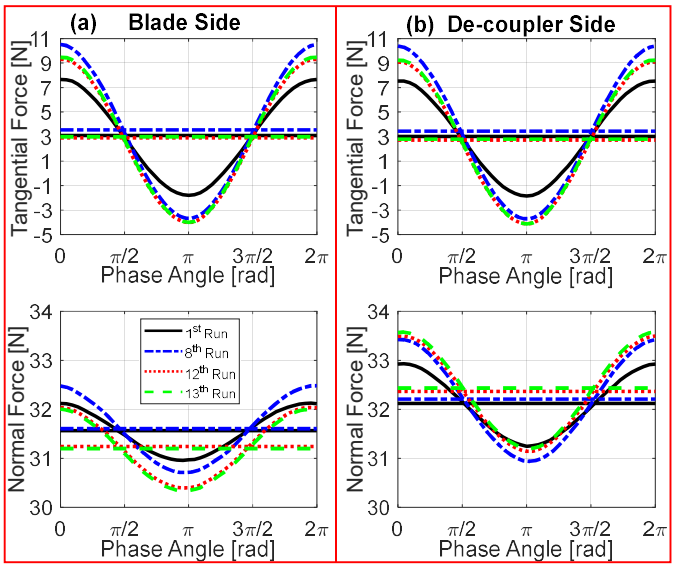

FIGURE 10: CONTACT FORCES ON THE RIGHT DAMPER FOR THE 4TH SUBSET (F_{EXC} = 5 N, CF = 6.6 kg)

TABLE 4: STATIC COMPONENTS OF CONTACT FORCES ON THE RIGHT DAMPER FOR THE 4TH SUBSET (F_{EXC} = 5 N, CF = 6.6 kg)

Runs	T'	N'	T''	N''	Resultant Force	
					X Dir.	Y Dir.
1st	3.01	32.12	3.1	31.56	0.0059	0.0014
8th	3.45	32.21	3.54	31.6	-0.0015	-0.0005
12th	2.73	32.36	2.89	31.24	-0.0079	-0.005
13th	2.8	32.43	2.98	31.2	-0.0044	0.0009

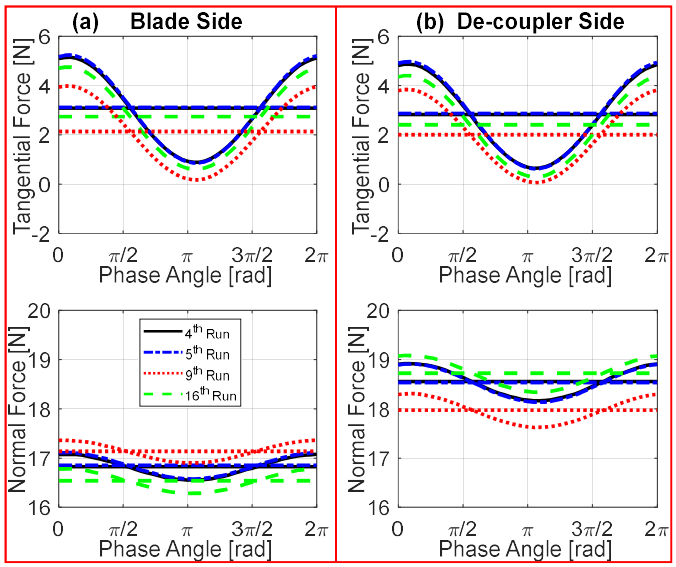

FIGURE 11: CONTACT FORCES ON THE RIGHT DAMPER FOR THE 3RD SUBSET (F_{EXC} = 1 N, CF = 3.6 kg)

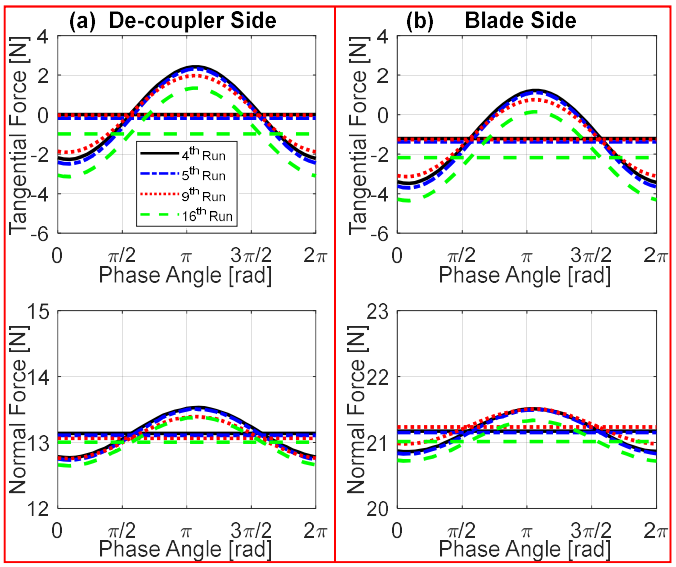

FIGURE 12: CONTACT FORCES ON THE LEFT DAMPER FOR THE 3RD SUBSET (F_{EXC} = 1 N, CF = 3.6 kg)

To make further investigations on the same phenomenon, the results measured in the 3rd subset (F_{EXC} = 1 N, CF = 3.6 kg) are given for the right damper in Figure 11. The response variability is also large for this case, as shown in Figure 6c. It can be seen in Figure 11 that the amplitudes of all forces in each subfigure is approximately equal; but, some of the static components of the tangential forces is again notably different than the other ones. In particular, the curves of the 4th and 5th runs exactly overlap; yet, the static tangential component of the 16th run is slightly different from them, while the one for the 9th run is considerably far. Like in the previous case, this pattern is also totally in-line with the response variability pattern, as shown in Figure 6c. On the other hand, contact forces at the left damper for the same subset is also given in Figure 12. Here, the curve measured in the 9th run breaks the trend, while the rest of the static tangential forces comply with the variability pattern. Nevertheless, it can be inferred that static component of the tangential forces is non-unique, which phsyically corresponds to different static force equilibria on the damper. This phenomenon accordingly causes the response variability, even though the results of one run is out of the common pattern presented in totally sixteen cases. As was similarly claimed in Section 3.1.1, this is the second observation supporting the hypothesis of [20, 21] which states that the non-repeateability of the nonlinear response is caused by the non-unique static component of the tangential force.

It can also be noted that there is an offset in the normal force values of de-coupler and blade sides at the left damper. This is probably resulted by a misalignment in the assembly, even though everything seemed properly aligned during the tests. It should be underlined that the entire structure is a complex system and it is composed of several subcomponents. The difficulties in the assembling procedures always create problems in laboratory conditions. Nevertheless, the contact forces and all other measurements are recorded in a reasonable and consistent manner, where the coherence of the results is ensured.

It is observed in the results of the investigated subsets that the non-uniqueness of static tangential forces creates a variability range in the nonlinear vibration amplitudes. These two subsets (the 3rd and 4th) are the ones with the largest variability range. Now, this observation is further challenged whether it will be still consistent with the results of the 6th subset (F_{EXC} = 5 N, CF = 3.6 kg). This case is intentionally selected, because it is the one where the response behavior is closest to a unique pattern with the highest repeatability (see Figure 6f). Figure 13 and Figure 14 illustrate the corresponding contact forces at the resonance frequency of each run for the right and left dampers, respectively. A similar variability pattern between the response and the static components of the tangential forces is also valid here. The behavior of three runs (the 4th, 5th and 16th runs) is similar to each other in both Figure 13 and Figure 6f, while the last one (the 9th run) is slightly different from them. In Figure 14, the curve of the 16th run becomes distant from the 4th and 5th ones, but the general pattern is still preserved.

All the results show that there are mutually strong compliances on the variability pattern of the response and the static component of the tangential forces, which shows a parallelism to the hypothesis of [20, 21]. This is also supported with other results in Section 3.1.1, in which it is shown that the range of the response variability is largely affected by the amount of micro slip motion occurring in the frictional surfaces. As a result, it can be understood that the response variability, measured in our experiments under the same nominal conditions, is mainly caused by the non-uniqueness of the static tangential components. These observations also verify the argument stated in [11], as mentioned in the introduction.

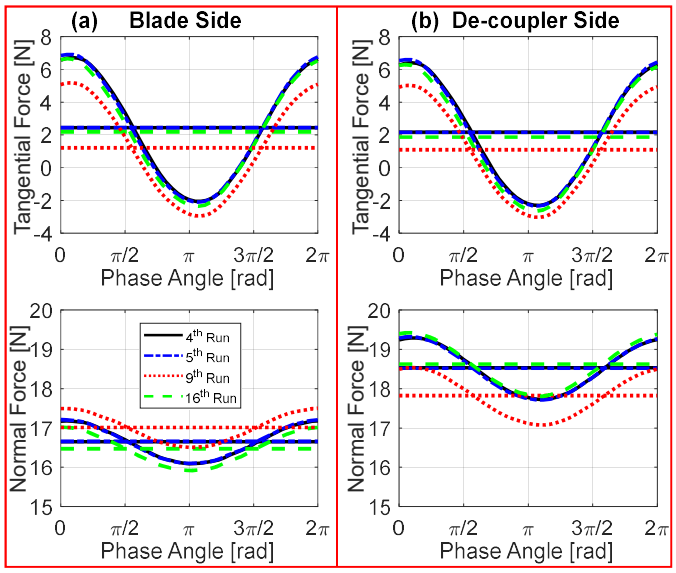

FIGURE 13: CONTACT FORCES ON THE RIGHT DAMPER FOR THE 6TH SUBSET (F_{EXC} = 5 N, CF = 3.6 kg)

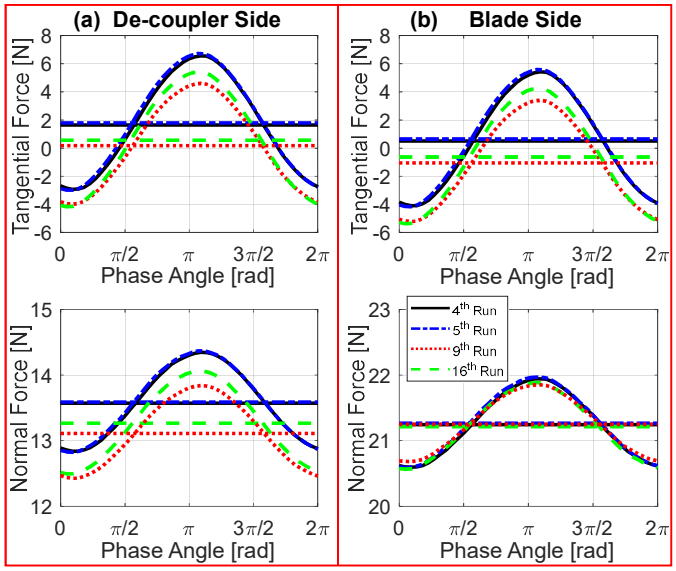

FIGURE 14: CONTACT FORCES ON THE LEFT DAMPER FOR THE 6TH SUBSET (F_{EXC} = 5 N, CF = 3.6 kg)

It is worth mentioning that other uncertainties may also be inevitably present in the nonlinear nature of the frictional systems, which may contribute to the response variation. For instance, tribological effects at the contact surfaces or dissimilar thermal expansion of different components may be relevant to change the micro conditions of frictional interfaces, even if macro scale conditions are nominally same. Moreover, some uncertainties may be physically connected to each other within the repeatability concept of systems with frictional structures. This research area is still highly active and requires further investigations to address all the concerns. In this study, their detailed investigation is out of scope, and the results are highly consistent with the uncertainty of the non-unique tangential forces.

3.3.4 The Evolution of the Contact Forces

It is shown that the achievement of the static force equilibria in different ways provides the variability in the nonlinear response. Monitoring the change of contact forces from beginning to the end of a frequency sweep gives an insight to visualize the entire process.

Figure 15 shows the measured contact forces at the de-coupler side of the right damper for the 4th subset that has the largest variability (F_{EXC} = 5 N, CF = 6.6 kg). The forces are measured for the entire frequency sweep in the 1st run that corresponds to the black response curve in Figure 6d. The evolution of the forces is shown for the dynamic and static components together. In this particular case, the sweep is performed from higher to lower frequencies. The amplitude of the dynamic part increases through the resonance, and then decreases with lowering frequencies. This behavior is expected, because the larger the vibration amplitudes, the higher the contact forces. However, it is interesting to note that the static part is not constant, and evolves in such a way that it directly decreases after starting the experiment, then slightly increases around the resonance region. After a certain point, it reaches to a saturation value at which it approximately remains the same until the end of the test. It should be noted that these contact forces are recorded in the 1st run, where the dampers had just been loaded with the dead weights. The change of the static components during frequency sweeps is a common behavior for initial runs performed after the dampers are loaded (1st and 9th runs). The data of all initial runs are not given here for brevity.

For the sake of comparison, the evolution of static contact forces, which corresponds to successive runs for the same sub-

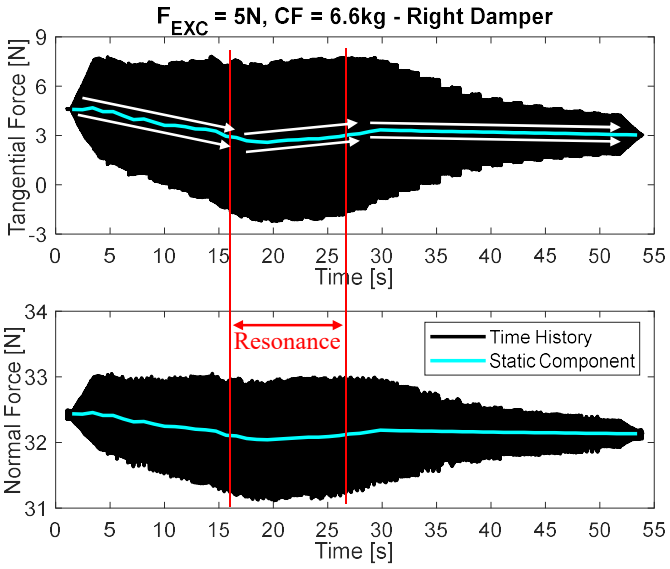

FIGURE 15: THE EVOLUTION OF THE CONTACT FORCES ON THE RIGHT DAMPER IN THE 1ST RUN OF THE 4TH SUBSET (F_{EXC} = 5 N, CF = 6.6 kg)

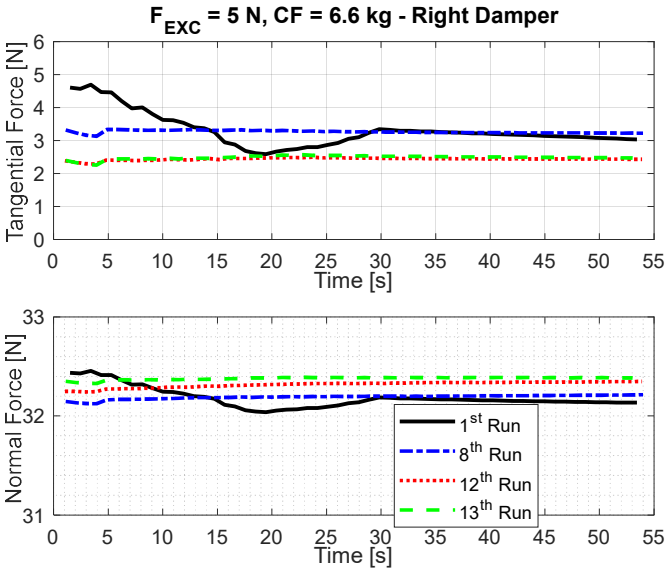

FIGURE 16: THE EVOLUTION OF STATIC CONTACT FORCES ON THE RIGHT DAMPER IN DIFFERENT RUNS FOR THE 4TH SUBSET (F_{EXC} = 5 N, CF = 6.6 kg)

set, is shown for the right and left dampers in Figure 16 and Figure 17, respectively. Unlike to the 1st run, the static components are almost constant throughout the entire sweep for the 8th, 12th and 13th runs where the dampers had been loaded before and some other runs have already been performed in advance. Hence, these results show that removing the damper and then reloading it back may somehow create different contact conditions, where the static balance may be mobile during the sweep. The main reason of this phenomenon cannot be fully revealed in the current study, since the exact contact conditions at the micro scale is a black box. However, we think

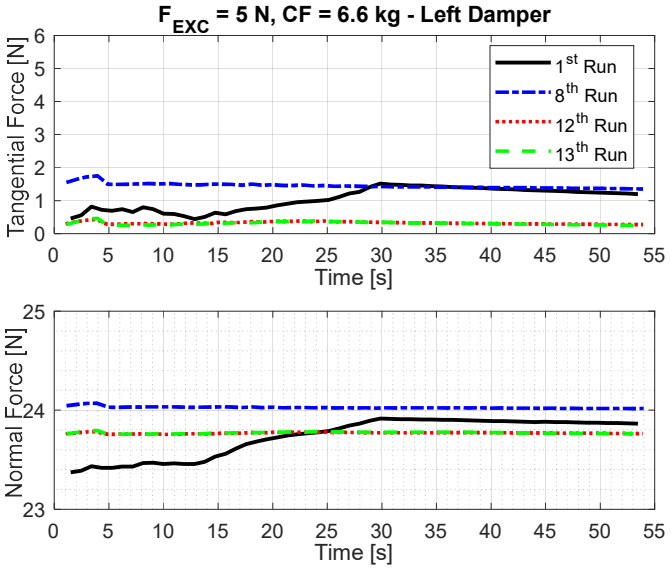

FIGURE 17: THE EVOLUTION OF STATIC CONTACT FORCES ON THE LEFT DAMPER IN DIFFERENT RUNS FOR THE 4TH SUBSET (F_{EXC} = 5 N, CF = 6.6 kg)

that the conformity of the asperities formed in the 1st runs continuously change during the micro slip around the resonance until a saturation point as the contact states approach to an almost fully stuck condition at the out-of-resonance. Then, in the seven successive runs, the final conformity of the 1st run is nearly maintained, since the damper is not removed; which enables a constant static force throughout the entire sweeps. This interpretation is also consistent with the so-called "bedding-in" phenomenon [22] which is referred to as the fact that a certain amount of time is needed during the tests until smooth surfaces are achieved in the frictional interfaces after starting the experiment. In the literature, this practice is popular to increase the repeatability of the nonlinear response. However, it should also be underlined that the variability phenomenon is not an error but a consequence of physical uncertainties present in the contact interfaces.

4. CONCLUSION

In this study, a novel test setup is designed to experimentally investigate the response variability of an academic turbine blade coupled with mid-span dampers. The non-repeatability of the vibration response is measured under the same nominal conditions but in different runs. A purposely defined testing strategy is applied to be able to modify the micro scale contact conditions, by ensuring that the user-controlled inputs are identical at the macro scale testing environment. To reveal the underlying kinematics of the frictional surfaces; contact forces, relative displacement between components and the rigid rotation of the damper are measured. It is shown with a large amount of data that the variability phenomenon is directly related to an uncertainty present in the friction forces, which enables different static force equilibria on the damper. The experimental results are consistent with the hypothesis of [20, 21], where the non-uniqueness of tangential forces provides the response variability.

It is also shown that the range of variability is larger when there is a dominating micro slip in the frictional surfaces. It decreases through the fully stuck or gross slip contact conditions. The difference between the multiple responses is larger in the amplitudes (10% - 60%) rather than the resonance frequencies (<1%). This indicates that the variability cannot be ignored, particularly in the amplitudes, and designers may become more aware about the variability phenomenon with this study.

REFERENCES

[1] Cowles, B. A. "High Cycle Fatigue in Aircraft Gas Turbines - An Industry Prospective." *Int. J. Fracture* Vol. 80 No. 2-3 (1996): pp. 147–163.

[2] Srinivasan, A. V. "Flutter and Resonant Vibration Characteristics of Engine Blades." *ASME J. Eng. Gas Turbines Power* Vol. 119 No. 4 (1997): pp. 742–775.

[3] Panning, L., Popp, K., Sextro, W., Gotting, F., Kayser, A., and Wolter, I., "Asymmetrical Underplatform Dampers in Gas Turbine Bladings: Theory and Application." *Proceedings*

of the ASME Turbo Expo 2004: Power for Land, Sea, and Air. Volume 6: Turbo Expo 2004. Vienna, Austria. June 14–17, 2004. pp. 269-280. ASME.

[4] Cigeroglu, E., An, N., and Menq, C. H. "Forced Response Prediction of Constrained and Unconstrained Structures Coupled Through Frictional Contacts." *ASME J. Eng. Gas Turbines Power* Vol. 131 No. 2 (2009): 022505.

[5] Laxalde, D., Thouverez, F., and Lombard, J. P. "Forced Response Analysis of Integrally Bladed Disks with Friction Ring Dampers." *J. Vib. Acoustics* Vol. 132 No. 1 (2010): 011013.

[6] Afzal, M., Lopez, A. I., and Kari, L. "Investigation of Damping Potential of Strip Damper on a Real Turbine Blade." *Proceedings of ASME Turbo Expo 2016: Turbomachinery Technical Conference and Exposition. Volume 7A: Structures and Dynamics.* Seoul, South Korea June 13–17, 2016. V07AT32A017. ASME.

[7] Denimal, E., Wong, C., Salles, L., and Pesaresi, L. "On the Efficiency of a Conical Underplatform Damper for Turbines." *ASME J. Eng. Gas Turbines Power* Vol. 143(2) (2021): 021020.

[8] Szwedowicz, J., Secall-Wimmel, T., and Dünck-Kerst, P. "Damping Performance of Axial Turbine Stages with Loosely Assembled Friction Bolts: The Nonlinear Dynamic Assessment." *ASME J. Eng. Gas Turbines Power* Vol. 130 No. 3 (2008): 032505.

[9] Drozdowski, R., Völker, L., Häfele, M., and Vogt, D. M. "Experimental and Numerical Investigation of the Nonlinear Vibrational Behavior of Steam Turbine Last Stage Blades with Friction Bolt Damping Elements." *Proceedings of ASME Turbo Expo 2015: Turbine Technical Conference and Exposition*. Montreal, Canada, June 15-19, 2015.

[10] Siewert, C., Sieverding, F., McDonald, W. J., Kumar, M., and McCracken, J. R. "Development of a Last Stage Blade Row Coupled by Damping Elements: Numerical Assessment of Its Vibrational Behavior and Its Experimental Validation During Spin Pit Measurements." *Proceedings of ASME Turbo Expo 2017: Turbomachinery Technical Conference and Exposition*. Charlotte, NC, USA, June 26-30, 2017.

[11] Ferhatoglu E., Zucca S., Botto D., Auciello J., and Arcangeli L., "Nonlinear Vibration Analysis of Turbine Bladed Disks with Midspan Dampers", *ASME J. Eng. Gas Turbines Power* Vol. 144(4) (2022): 041021.

[12] Mulvihill, D. M., Kartal, M. E., Nowell, D., and Hills, D. A., "An Elastic–Plastic Asperity Interaction Model for Sliding Friction." *Tribology International* Vol. 44 No. 12 (2011): 1679-1694.

[13] Eriten, M., Polycarpou, A. A., and Bergman, L. A. "Surface Roughness Effects on Energy Dissipation in Fretting Contact of Nominally Flat Surfaces." *ASME. J. Appl. Mech.* Vol. 78 No. 2 (2011): 021011.

[14] Butlin, T., Spelman, G., Ghaderi, P., Midgley, W.J.B., and Umehara, R., "Predicting Response Bounds for Friction-Damped Gas Turbine Blades with Uncertain Friction Coupling. *J. Sound and Vib.* Vol. 440 (2019): pp.399-411.

[15] Yuan, J., Fantetti, A., Denimal, E., Bhatnagar, S., Pesaresi, L., Schwingshackl, C., and Salles, L., "Propagation of Friction Parameter Uncertainties in the Nonlinear Dynamic Response of Turbine Blades With Underplatform Dampers." *Mech. Syst. Signal Process.* Vol. 156 (2021): 107673.

[16] Brake, M. R. W., Schwingshackl, C. W., and Reuß, P. "Observations of Variability and Repeatability In Jointed Structures." *Mech. Syst. Signal Process.* Vol. 129 (2019): 282-307.

[17] Sanliturk, K.Y., Ewins, D.J., and Stanbridge, A.B., "Underplatform Dampers for Turbine Blades: Theoretical Modeling, Analysis, and Comparison with Experimental Data." *J. Eng. Gas Turbines Power*, Vol. 123 No. 4 (2001): pp.919-929.

[18] Pesaresi, L., Salles, L., Jones, A., Green, J.S., and Schwingshackl, C.W., "Modelling the Nonlinear Behaviour of an Underplatform Damper Test Rig for Turbine Applications." *Mech. Syst. Signal Process.* Vol. 85 (2017): pp.662-679.

[19] Botto, D., and Umer, M., "A Novel Test Rig to Investigate Under-Platform Damper Dynamics." *Mech. Syst. Signal Proc*. Vol. 100 (2018): pp. 344-359.

[20] Yang, B.D., and Menq, C.H., "Characterization of Contact Kinematics and Application to the Design of Wedge Dampers in Turbomachinery Blading: Part 2—Prediction of Forced Response and Experimental Verification." *J. Eng. Gas Turbines Power*, Vol. 120 No. 2 (1998): pp.418-423.

[21] Ferhatoglu, E., and Zucca, S., "On the Non-Uniqueness of Friction Forces and the Systematic Computation of Dynamic Response Boundaries for Turbine Bladed Disks with Contacts." *Mech. Syst. Signal Proc*. Vol. 160 (2021): 107917.

[22] Sever, I. A., Petrov, E. P., and Ewins, D. "Experimental and Numerical Investigation of Rotating Bladed Disk Forced Response Using Underplatform Friction Dampers." *ASME J. Eng. Gas Turbines Power* Vol. 130(4) (2008): 042503.